Journal of the Optical Society of America B
OPTICAL PHYSICS

Tuning parametric processes in semiconductor diode lasers

Nima Zareian,[1] Dongpeng Kang,[2] and Amr S. Helmy[1,*]

[1]Edward S. Rogers Department of Electrical and Computer Engineering, University of Toronto, Toronto, ON M5S 3G4, Canada
[2]Currently at School of Astronautics and National Key Laboratory of Science and Technology on Tunable Laser, Harbin Institute of Technology, 92 West Dazhi Street, Harbin 150001, China
*Corresponding author: a.helmy@utoronto.ca

Received 14 December 2017; accepted 4 January 2018; posted 9 January 2018 (Doc. ID 315664); published 9 February 2018

We present GaAs/AlGaAs semiconductor lasers in which second-order nonlinearities are phase matched for efficient second-order nonlinear conversion. A comprehensive study of difference frequency generation (DFG) is presented, and the process is characterized for tuning, efficiency, and tolerances. External nonlinear conversion efficiency of $1.84 \times 10^{-2}\,\%/\mathrm{W}/\mathrm{cm}^2$ is measured for the DFG process. The effects of carrier injection and temperature variation on DFG wavelength are studied, and the two effects are deconvolved for better understanding of carrier effects on nonlinear conversion. A wide DFG tuning range for the device operation is experimentally demonstrated where the idler wavelength can be tuned more than 30 nm for every 1-nm span of the pump wavelength.

OCIS codes: (190.4390) Nonlinear optics, integrated optics; (190.4410) Nonlinear optics, parametric processes; (250.5960) Semiconductor lasers.

https://doi.org/10.1364/JOSAB.35.000552

1. INTRODUCTION

Ultra-fast parametric processes play a pivotal role in enabling a photonic device library with a wide spectrum of functions, particularly in semiconductors. These processes provide a range of optical effects including gain, frequency conversion, nonlinear phase, and absorption. While the third-order nonlinearity is the most utilized type of ultrafast nonlinearity in monolithic semiconductors, the second-order nonlinearity has also been recently harnessed in this platform [1–5]. Utilizing third-order nonlinearity is easier in semiconductors due to their relaxed phase-matching conditions. Due to the substantial dispersion associated with semiconductors when operating near the bandgap, phase matching proves challenging for their second-order counterparts, however.

Bragg reflection waveguides (BRWs) have recently received increasing attention as an attractive architecture for efficient second-order nonlinear interactions. Nonlinear conversion in semiconductor devices such as BRWs provides a compact platform for parametric devices in an integrated setting. Recently, parametric generation and nonlinear conversion have been demonstrated in this platform [1–4,6–8]. Bragg reflection waveguide lasers (BRLs) have also been demonstrated [9] and used for self-pumped spontaneous parametric down-conversion (self-pumped SPDC) [9–11]. Self-pumped difference frequency generation (DFG) in BRLs promises monolithically integrated, widely tunable sources of coherent radiation at room temperature. In a self-pumped DFG process, the pump can be generated via on-chip lasing, achieved through band-to-band recombination in quantum wells, for example, while an external signal can be injected into the device. Through nonlinear mixing of signal and pump the idler is generated, with wavelength tunability dictated by the dispersion of the structure and the associated materials. In a self-pumped SPDC process, the pump is similarly generated via on-chip lasing, achieved through band-to-band recombination, and is then parametrically down-converted into a signal and idler within the same cavity [9].

Nonlinear conversion tuning and tolerances have been well studied in passive nonlinear integrated devices [3,4] where the temperature of the structure is the chief cause of drift in the phase-matching wavelength. In a self-pumped DFG or SPDC process, however, both carrier injection and heat generation within the device will modify the material characteristics and tune the phase-matching wavelength as well as the wavelength of the pump that is generated within the structure. As progress is made in self-pumped nonlinear conversion in integrated devices, these intra-cavity tuning effects become more important as they provide a critical path for device design. Since self-pumped BRL devices were first reported a few years ago [11,12], carrier and temperature effects have not yet been well studied. As such, studying the changes in phase matching and on-chip pump wavelength due to these

effects is essential in enabling optimal design of self-pumped parametric devices.

In reports on self-pumped SPDC and parametric fluorescence in GaAs/InGaAs BRLs [12,13], the pump wavelength is modified through tuning the injected current so as to obtain a parametric fluorescence tuning curve. While using such an approach can provide a tuning curve, the changes in the signal and idler wavelength may be attributed to multiple factors. Those include carrier-induced index variation, temperature variation, and changes in the pump wavelength. Even though a relation between the pump wavelength and signal/idler wavelength can be established, these studies do not experimentally determine what roles the change in pump wavelength, modification of device temperature, and current play in shaping the tuning curve. A more recent study, which reported self-pumped SPDC in GaAs/AlGaAs BRLs [11], was focused primarily at the photon pair generation, and hence the dependence of conversion process on the cavity parameters was not reported.

In this paper, we investigate DFG in electrically injected BRLs and its tuning characteristics with temperature and injected current. The information presented is extremely important for implementation of self-pumped DFG and self-pumped SPDC in GaAs/AlGaAs diode lasers. Using an external pump while tuning the current injection enables us to study the free carrier effects on the DFG phase-matching condition without the concomitant effect of having the pump wavelength change. The effect of cavity temperature change on the conversion process is also investigated. This is the first time to our knowledge that the impacts of these factors have been experimentally studied and separated in semiconductor lasers.

This paper is organized as follows. In Section 2, the device design and lasing performance are described. The DFG performance is then examined using external pump injection in Section 3. Such an approach enables us to separate the effect of current injection and pump wavelength tuning, which will be used in Section 4 for characterizing the effect of temperature and carrier injection on the DFG phase-matching condition.

2. LASER DESIGN AND PERFORMANCE

The BRL structure studied in this work is a *p-i-n* GaAs/AlGaAs Bragg waveguide. The second-order nonlinearity in this structure is phase matched for DFG with a pump wavelength around 816 nm and signal and idler wavelengths around 1550 nm and 1700 nm, respectively. The device is designed for lasing in the Bragg mode around 785 nm, well away from the pump wavelength, which facilitates DFG measurement with external injection at the same time that the laser is electrically driven. Examining the conversion process by employing an external source allows for both pump and signal wavelength to be tuned without affecting other properties. As such, the isolated effect of each parameter on the nonlinear conversion can be determined and investigated easily.

The wafer was grown on 2°-off [001] *n*-type GaAs using metal-organic chemical vapor deposition (MOCVD). The design includes upper and lower transverse Bragg reflectors of 4 and 5 periods of $Al_{0.70}Ga_{0.30}As/Al_{0.25}Ga_{0.75}As$, respectively. A matching layer composed of $Al_{0.20}Ga_{0.80}As$ is utilized on either side of the core. The core is composed of $Al_{0.70}Ga_{0.30}As$. Two InAlGaAs quantum wells and three $Al_{0.28}Ga_{0.72}As$ barriers are placed within the core. Finally, a GaAs cap layer is placed on top of the structure. The Bragg reflectors are doped with a gradient from 1×10^{-17} cm^{-3} to 3×10^{-18} cm^{-3}. Figure 1 illustrates refractive index profile of the structure as well as the mode profiles of the 1D slab waveguide at the pump, signal, and idler wavelengths.

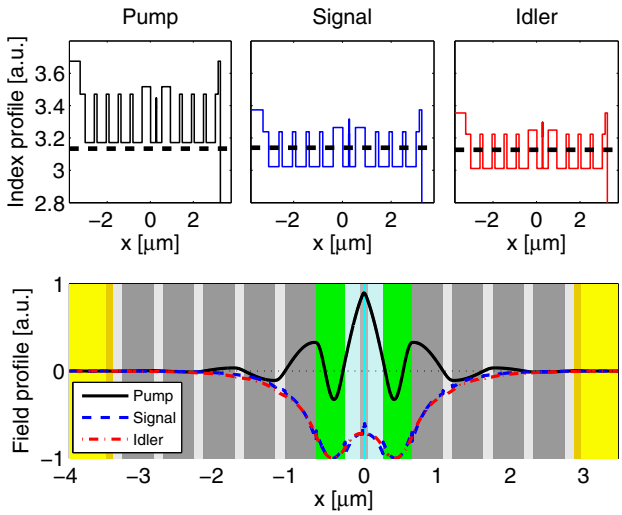

Fig. 1. Refractive index profile at pump, signal, and idler wavelengths, i.e., 816, 1550, and 1723 nm (top), and schematic and mode profile of the structure (bottom). The dashed black lines in the index profile represent the effective index.

Ridge lasers were fabricated with ridge widths of 2 μm and etch depths ranging between 1.8 and 2.2 μm. E-beam lithography, together with plasma etching, formed the ridges, while gold-alloy metal junctions formed the contacts. Lasers are then cleaved into individual bars with lengths varying between 500 and 1500 μm. Those are then mounted epi-side up on a copper block for characterization. Figure 2 shows a scanning electron micrograph (SEM) of a device after cleaving.

Figure 3(a) illustrates the power and voltage characteristics of two representative devices as a function of injected current, operated continuous wave (CW) at 20°C. Typical values for the threshold current density were measured to be 1705 A/cm^2

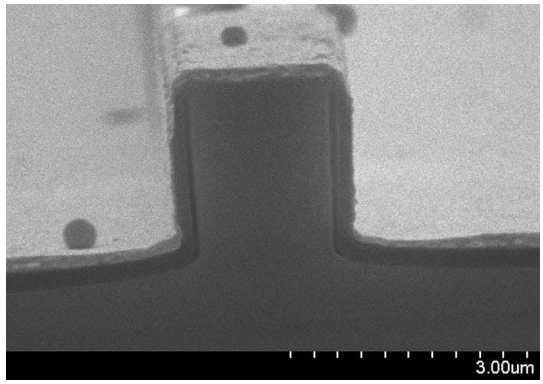

Fig. 2. SEM micrograph of a sample laser diode.

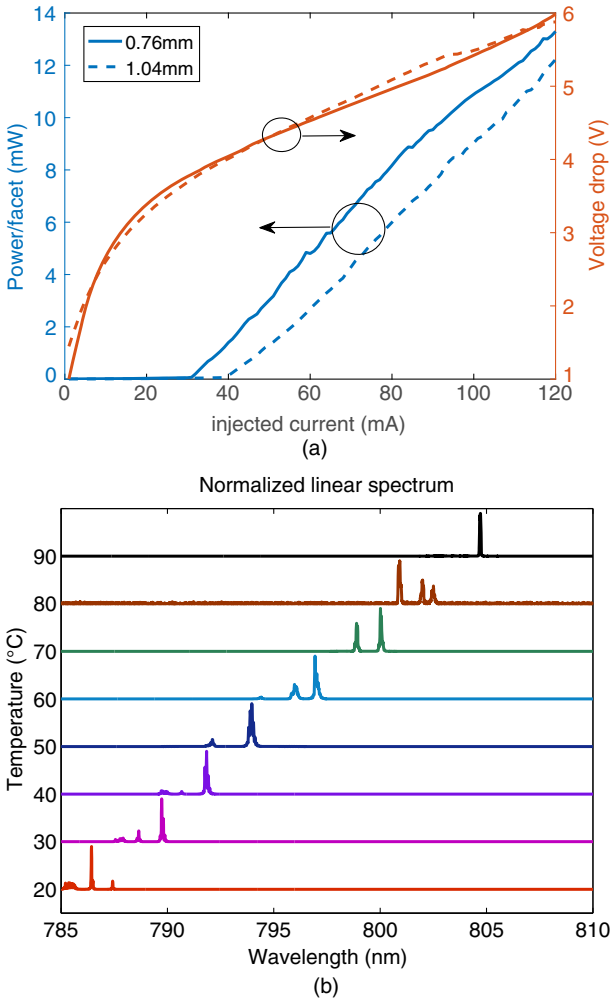

Fig. 3. (a) LIV curves for two diode lasers operated at 20°C. The solid and dashed lines represent a 0.76-mm-long and 1.04-mm-long device, respectively. (b) Normalized optical spectrum of the laser under test at 100 mA at various stage temperatures.

and 1615 A/cm^2 for the 1.04-mm-long and 0.76-mm-long devices, respectively. The observed threshold current density is within the range of values that was reported previously for similar devices [9,11], but rather higher than state-of-the-art diode lasers in the same material system. This larger threshold current density can be attributed to the design trade-offs for the nonlinear conversion, such as the larger loss of Bragg mode compared to the conventional TIR mode. As the current laser is designed for nonlinear conversion, the laser efficiency was given up in part in exchange for efficient conversion efficiency. Some of the design trade-offs in designing such structures were discussed previously [10]. The modal propagation loss was measured to be 14.3/cm using the cut back method [14]. This loss value is larger than typical values measured for similar devices [15,16]. This is in part due to the extensive reach of the optical field of the Bragg mode within the cladding, which yields to larger overlap with the doped layers. This extended field offers higher nonlinear conversion efficiency [10]. Figure 3(a) also shows the voltage drop of the devices with injected current. The threshold voltage drop on the devices

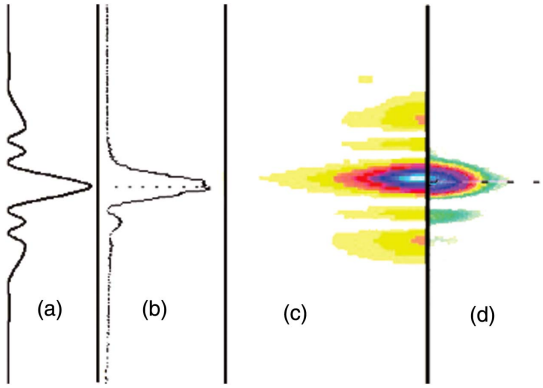

Fig. 4. Near field of the laser under test at 20°C and 100 mA current. (a) Calculated and (b) measured 1D NF profile. (c) Calculated and (d) measured 2D NF profile.

is nearly 3.2 V. This rather large voltage drop across the devices is due to the sub-optimal doping of the Bragg stacks. Optimization of the doping profile and use of delta-doping would lead to lower device resistance.

Figure 3(b) shows the emission optical spectra of the long laser operated CW at 100 mA for temperatures ranging from 20°C to 90°C. As the device is biased well above the threshold current, the optical spectrum shows multiple peaks. Nevertheless, the center wavelength of the major peak can be roughly associated with the gain peak and can be studied as a function of temperature. A net shift of 0.261 nm/°C is observed in the measured peak wavelength, which is in line with the expected temperature-dependent shift in the bandgap. In addition, the effect of current on junction temperature is measured using [17] to be 0.11°C/mA. This value is directly dependent on heatsinking of the device and its thermal resistance. As such, the effect cannot be verified with other similar measurements in the literature. These measured net thermal effects will be used in the next section to separate the effect of temperature and carriers in the device performance.

In order to confirm that lasing takes place for the intended Bragg mode, the near-field profile of the laser is measured as shown in Fig. 4. The calculated theoretical predictions are also given in the same figure to demonstrate the correspondence of the results. The near field preserves its shape throughout the entire range of tested bias currents up to four times the threshold current.

3. DFG PERFORMANCE

To investigate nonlinear properties of the device, a type-II DFG measurement is carried out on a BRL with a length of 1.04 mm. For this experiment, the diode laser was not electrically injected, and external pump and signal sources were used. A CW tunable external cavity laser source (JDSU SWS15101) is amplified using an erbium-doped fiber amplifier (Amonics AEDFA series) and passed through a tunable filter to reject the background spontaneous emission at the unwanted wavelengths. The signal obtained is then mixed with the pump from a CW tunable Ti:Sapphire laser (Coherent MBR series) through a beam splitter and end-fire coupled into the device

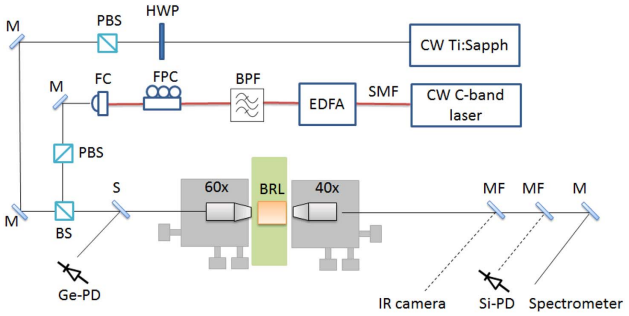

Fig. 5. Schematic of DFG experimental setup. Two tunable sources emitting around 816 nm and 1550 nm wavelength are injected into the sample after beam shaping and polarization control. SMF, single mode fiber; BPF, tunable band-pass filter; FPC, fiber polarization controller; FC, fiber collimator; PBS, polarization beam splitter; BS, beam splitter; S, beam sampler; M, mirror; MF, flip-mount mirror; BRL, Bragg reflection waveguide laser; Ge-PD, germanium photodetector.

using an antireflection-coated 60× objective lens. For the signal beam path, a fiber polarization controller and polarization beam splitter are used to manipulate the signal polarization. For the pump beam path, a half-wave plate and polarization beam splitter are used in the optical path, allowing for the required linear polarization to pass through. At the sample output, the idler is collected with a 40× objective lens and then passed through a free-space spectrometer (Horiba iHR320). The spectrometer is equipped with a lock-in amplifier (SRS830) and a sensitive strained InGaAs detector (EOS IGA2.2-010-TE2-H). The lock-in amplifier helps reduce the noise floor, which, together with the sensitive detector, allows us to measure the sub-nanowatt (nW) idler powers. A schematic of the setup is shown in Fig. 5.

The signal/pump are set to 21 mW/90 mW power in the transverse magnetic (TM)/transverse electric (TE) polarization, and the idler spectrum is recorded for various pump wavelengths. Both the signal and pump wavelengths are swept over a suitable range, input power is kept constant, and the pump/signal wavelength combinations corresponding to the maximum idler power are recorded together with the idler peak wavelength. Figure 6(a) shows the measured DFG tuning curve illustrating an idler wavelength tuning range of more than 30 nm with a change of less than 1 nm in the pump wavelength. This demonstrates the very wide tuning range attainable in self-pumped DFG BRLs.

Due to the proximity of signal and idler wavelengths and the large difference between the power levels, separation of the signal and idler waves at the waveguide output is challenging. As such, the idler power is estimated by carefully calibrating the spectrometer data. The dependence of the calibrated idler power on pump wavelength for a constant signal wavelength of 1550 nm and signal/pump power of 21 mW/90 mW is shown in Fig. 6(b). A peak idler power of 1.82 nW is obtained for the phase-matched pump at 816.3 nm. The bandwidth of the process is found to be 0.74 nm. The inset shows the linear relation of idler power with product of pump and signal powers for pump/signal wavelength of 816.3/1550 nm. The external DFG normalized conversion efficiency is estimated to be $1.84 \times 10^{-2}\%/\mathrm{W}/\mathrm{cm}^2$, taking into account a 70% objective

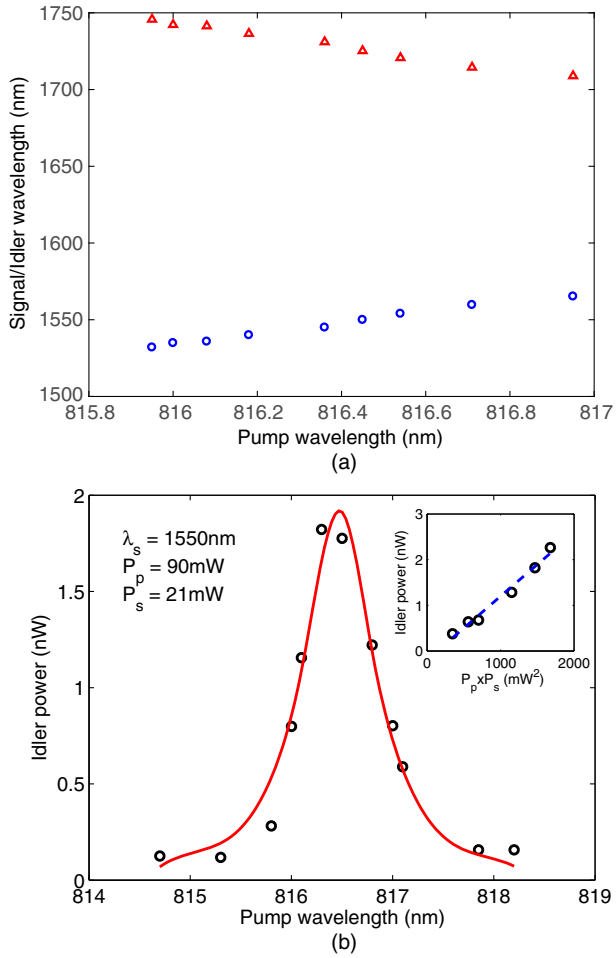

Fig. 6. (a) Measured DFG tuning curve of the device under test. The circles highlight the signal wavelength and triangles represent the idler. (b) Idler power plotted against pump wavelength for a constant signal wavelength of 1550 nm. The circles are the measured data and the solid line shows a Lorentzian fit. Inset shows the idler power plotted as a function of signal power for a constant pump power of 90 mW. The dashed line is a linear fit.

lens collection efficiency for the idler. The conversion efficiency measured in these device compared well with previously reported passive devices. The device conversion efficiency is comparable with those reported for DFG in similar passive structures [2], and nearly three times larger than those estimated for SHG in similar active structures [11]. While this confirms the efficiency of the procedure for designing the doped structure, note that the measured conversion efficiency is reported without carrier injection.

4. TUNING THE DFG WAVELENGTH

The experimental determination of thermal and carrier effects on phase matching is essential for understanding the device performance and future implementation of self-pumped DFGs in similar structures. Here, the dependence of the DFG phase-matching wavelength on temperature and injected current is investigated using the same device to provide a full map of device spectroscopy.

To study the effect of temperature, essentially the same experiment as the previous section is carried out at various stage temperatures, that is, DFG with externally injected pump and signal and no electrical injection. A temperature-controlled stage is used to hold the sample temperature at 10°C–100°C with steps of 10°C. The signal and pump are mixed in a 50/50 fiber splitter/combiner, and the output is injected into the sample through a cleaved facet fiber. The output is collected through a 40× objective lens, and the idler power is spectrally resolved using the spectrometer, similar to the previous experiment. For every temperature point, the pump wavelength is tuned while recording the idler power, and the wavelength corresponding to the peak power is recorded as the phase-matching wavelength. Signal wavelength is kept constant at 1550 nm throughout this experiment, and the pump/signal power is kept at 18/40 mW. As shown in Fig. 7(a), temperature tuning can vary the phase-matching wavelength by $\Delta\lambda/\Delta T = 0.1$ nm/°C. This will provide vital insight into the future device designs by taking the effect of temperature on both lasing and phase-matching wavelengths into account.

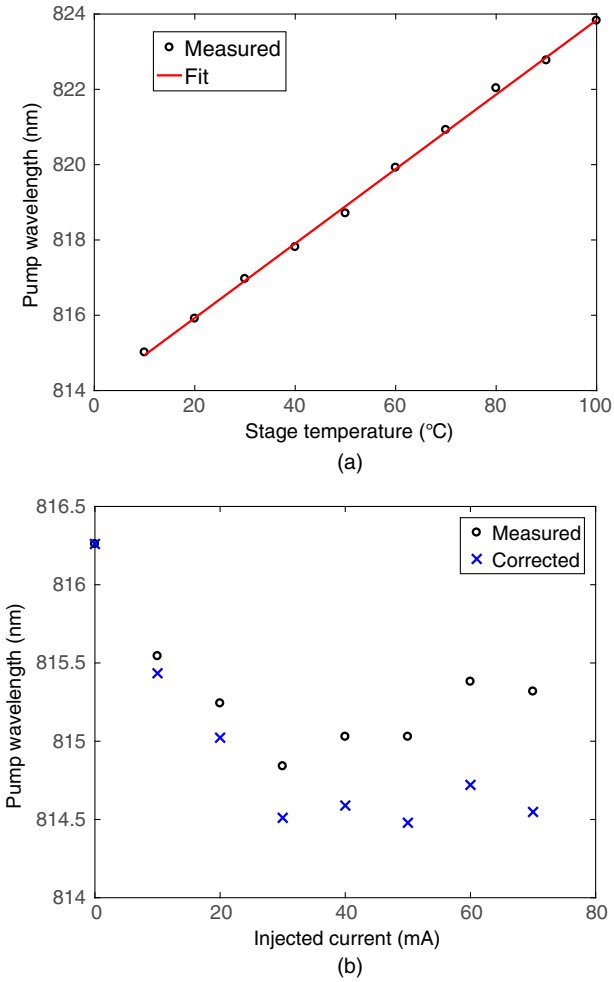

Fig. 7. DFG phase-matching wavelength for constant signal wavelength of 1550 nm, plotted as a function of (a) stage temperature and (b) injected current. In the latter figure, stage temperature was kept constant at 20°C.

Injection of free carriers into the device active region can also modify the quantum well material refractive index by up to a few percent [18]. Depending on the conditions, such a change can correspond to a blueshift of as much as tens of nanometers in the phase-matching wavelength in GaAs/AlGaAs devices. The effect of carrier injection on the phase-matching wavelength can be documented by measurement of phase-matching wavelength at various injection currents at a constant stage temperature. Keeping the signal wavelength constant allows for deconvolving the thermal effects of current injection on the phase-matching wavelength from the carrier effects without introduction of any additional variables. The DFG phase-matching wavelength is investigated while the CW current is injected into the sample through two gold-plated copper probes at a constant 20°C stage temperature. Once more the signal wavelength is kept constant at 1550 nm, the externally injected pump wavelength is tuned, and the idler power is monitored for a range of injected current levels of 0–90 mA with a step of 10 A. The phase-matching wavelength was recorded and plotted as black circles in Fig. 7(b) over the tested currents. The figure shows less than 2-nm blueshift in the phase-matching wavelength through current injection.

Even though the stage temperature is kept constant, the device junction temperature can increase significantly due to carrier injection. In the current case, the redshift in phase-matching point caused by the increase in junction temperature is offsetting the phase-matching wavelength blueshift caused by carrier injection. As the effect of current injection on junction temperature is known from the previous section, effect of carrier injection and junction temperature can be deconvolved to study the sole effect of carrier injection on the phase-matching wavelength. To do this, the temperature effects have to be calculated, and the phase-matching point should be offset by the calculated value so as to only represent the effect of carrier injection on the phase-matching wavelength. The corrected DFG phase-matching wavelength can be calculated based on the following equation:

$$\lambda_{\mathrm{PM,corrected}} = \lambda_{\mathrm{PM}} - \Delta\lambda/\Delta T \times \Delta T/\Delta I \times I. \quad \textbf{(1)}$$

Here λ_{PM} is the measured pump phase-matching wavelength, $\lambda_{\mathrm{PM,corrected}}$ is the corrected phase-matching wavelength, $\Delta\lambda/\Delta T$ is the slope of the phase-matching wavelength versus temperature curve (0.1 nm/°C), $\Delta T/\Delta I$ represents the effect of junction temperature on bias current (0.11°C/mA), and I is the diode laser bias current. Both $\Delta\lambda/\Delta T$ and $\Delta T/\Delta I$ were carefully measured and reported in the previous section. For each one of the measured bias points, the corrected phase-matching wavelength was calculated to only reflect the carrier injection effect. The resulting corrected phase-matching wavelength is plotted in Fig. 7(b) along with the DFG phase-matching wavelength. The difference between the corrected and measured values is essentially the redshift effect of junction temperature on the phase-matching wavelength. The linear blueshift of the corrected phase-matching wavelength below the laser threshold can be ascribed to the linear ascend of carrier concentration in the active region with the current. Above the threshold, however, carrier density is not linearly dependent on current injection, and the excess carriers are mainly consumed through radiative and nonradiative recombination. This trend

is clearly confirmed in the figure where the corrected phase-matching wavelength remains nearly unchanged above the threshold current. The effect of injected current on the phase-matching wavelength is estimated to be 76 pm/mA under the threshold and insignificant above the threshold. Based on this and our model, the index change rate as a function of carrier density was roughly estimated as 5e–21 cm^3, which is close to that previously reported in the literature [18].

5. CONCLUSION

Bragg reflection waveguide lasers were reported in which second-order nonlinearity is phase matched for efficient frequency conversion. The devices examined and characterized for DFG using a pump at 816 nm, signal at 1550 nm, and an idler at 1720 nm. The external nonlinear conversion efficiency was measured to be $1.84 \times 10^{-2}\%/W/cm^2$, which is close to the highest values previously reported for other similar passive and active devices. A wide DFG tuning range for the device operation was experimentally demonstrated where the idler wavelength can be tuned more than 30 nm by sweeping the pump wavelength by only 1 nm.

As the measured DFG degeneracy point is far from the lasing wavelength, it was possible to study the effect of temperature and current on tuning the phase-matching wavelength. In line with theoretical predictions, it was shown that while the DFG phase-matching wavelength changes linearly with temperature, carrier injection only tunes the phase-matching wavelength at currents below the laser threshold. This investigation of temperature and carrier effects on the phase-matching wavelength is the first systematic investigation to our knowledge of DFG phase-matching wavelength tuning reported in the literature and will play a pivotal role in judicious design of future parametric devices based on semiconductor laser cavities.

Funding. Natural Sciences and Engineering Research Council of Canada (NSERC); CMC Microsystems (CMC).

Acknowledgment. The authors thank CMC Microsystems for facilitating the wafer growth and microfabrication.

REFERENCES

1. P. Abolghasem, J. Han, B. J. Bijlani, A. Arjmand, and A. S. Helmy, "Highly efficient second-harmonic generation in monolithic matching layer enhanced AlxGa1-xAs Bragg reflection waveguides," IEEE Photon. Technol. Lett. **21**, 1462–1464 (2009).
2. J.-B. Han, P. Abolghasem, D. Kang, B. J. Bijlani, and A. S. Helmy, "Difference-frequency generation in AlGaAs Bragg reflection waveguides," Opt. Lett. **35**, 2334–2336 (2010).
3. B. Bijlani, P. Abolghasem, and A. S. Helmy, "Second harmonic generation in ridge Bragg reflection waveguides," Appl. Phys. Lett. **92**, 101124 (2008).
4. J. Han, P. Abolghasem, B. J. Bijlani, and A. S. Helmy, "Continuous-wave sum-frequency generation in AlGaAs Bragg reflection waveguides," Opt. Lett. **34**, 3656–3658 (2009).
5. P. Sarrafi, E. Y. Zhu, B. M. Holmes, D. C. Hutchings, S. Aitchison, and L. Qian, "High-visibility two-photon interference of frequency-time entangled photons generated in a quasi-phase-matched AlGaAs waveguide," Opt. Lett. **39**, 5188–5191 (2014).
6. R. T. Horn, P. Kolenderski, D. Kang, P. Abolghasem, C. Scarcella, A. Della Frera, A. Tosi, L. G. Helt, S. V. Zhukovsky, J. E. Sipe, G. Weihs, A. S. Helmy, and T. Jennewin, "Inherent polarization entanglement generated from a monolithic semiconductor chip," Sci. Rep. **3**, 2314 (2013).
7. D. Kang, A. Anirban, and A. S. Helmy, "Monolithic semiconductor chips as a source for broadband wavelength-multiplexed polarization entangled photons," Opt. Express **24**, 15160–15170 (2016).
8. D. Kang, M. Kim, H. He, and A. S. Helmy, "Two polarization-entangled sources from the same semiconductor chip," Phys. Rev. A **92**, 013821 (2015).
9. B. J. Bijlani and A. S. Helmy, "Bragg reflection waveguide diode lasers," Opt. Lett. **34**, 3734–3736 (2009).
10. B. J. Bijlani and A. S. Helmy, "Design methodology for efficient frequency conversion in Bragg reflection lasers," J. Opt. Soc. Am. B **29**, 2484–2492 (2012).
11. F. Boitier, A. Orieux, C. Autebert, A. Lemaître, E. Galopin, C. Manquest, C. Sirtori, I. Favero, G. Leo, and S. Ducci, "Electrically injected photon-pair source at room temperature," Phys. Rev. Lett. **112**, 183901 (2014).
12. B. J. Bijlani, P. Abolghasem, and A. S. Helmy, "Semiconductor optical parametric generators in isotropic semiconductor diode lasers," Appl. Phys. Lett. **103**, 091103 (2013).
13. B. J. Bijlani, P. Abolghasem, and A. S. Helmy, "Intracavity parametric fluorescence in diode lasers," in *CLEO: 2011—Laser Applications to Photonic Applications* (Optical Society of America, 2011), paper PDPA3.
14. H. C. Casey and M. B. Panish, *Heterostructure Lasers Pt.A. Fundamental Principles* (Academic, 1978).
15. B. Pressl, T. Günthner, K. Laiho, J. Geßler, M. Kamp, S. Höfling, C. Schneider, and G. Weihs, "Mode-resolved Fabry–Perot experiment in low-loss Bragg-reflection waveguides," Opt. Express **23**, 33608–33621 (2015).
16. C. Autebert, G. Maltese, Y. Halioua, F. Boitier, A. Lemaître, M. Amanti, C. Sirtori, and S. Ducci, "Electrically injected twin photon emitting lasers at room temperature," Technologies **4**, 24 (2016).
17. T. Paoli, "A new technique for measuring the thermal impedance of junction lasers," IEEE J. Quantum Electron. **11**, 498–503 (1975).
18. J. Mendoza-Alvarez, F. Nunes, and N. Patel, "Refractive index dependence on free carriers for GaAs," J. Appl. Phys. **51**, 4365–4367 (1980).